Quantification of Urban Heat Island Effect and Differences in Regional Influence Based on Footprint Analysis: A Case Study of the Beijing–Tianjin–Hebei Urban Agglomeration

Huisheng Yu and Dongqi Sun

***Abstract*—Extreme heat events occur frequently in urban areas, seriously affecting human well-being and productivity. Therefore, this article aimed to quantify the impact of and regional differences in the urban heat island (UHI) effect within the broader context of achieving sustainable development goals. To this end, we combined footprint analysis with principal component analysis and multivariate linear regression analysis to quantify the spatiotemporal distribution of heat island intensity and footprint within the Beijing–Tianjin–Hebei urban agglomeration as well as the impact of regional differences. We found that the surface urban heat island intensity (SUHII) value was higher during the daytime than at night. In 2005, 2010, 2015, and 2018, the average daytime values of SUHII were 0.21°C, 0.03°C, 0.35°C, and 0.53°C higher than those at night, respectively. High daytime values of SUHII mainly occurred in larger cities (e.g., Beijing), and high nighttime values of SUHII mainly occurred at higher latitudes. In addition, we determined that the maximum values of the SUHIF were concentrated in densely populated areas such as Beijing, Tianjin, and Shijiazhuang. Furthermore, principal component analysis revealed that PM2.5 was negatively correlated with SUHII, whereas population density (PD) and enhanced vegetation index were positively correlated with SUHII. In contrast, PM2.5 and EVI were negatively correlated with SUHIF, whereas PD and SUHIF showed a negative correlation. This article elucidates the changes in and influencing mechanisms of the UHI intensity and footprint and provides an important reference for mitigating the UHI effect and rationally planning urban land use.**

***Index Terms*—Driving factors, land surface temperature (LST), thermal environment, urban agglomeration, urban heat island (UHI) footprint.**

I. Introduction

SINCE the 21st century, global urbanization has accelerated. According to the China Statistical Yearbook, the proportion of the urban population in 2020 was 63.89%, an increase of 27.67% compared with that in 2000. And according to the 2020 World Cities Report, the urban population worldwide is expected to exceed 60% by 2030 [1]. Concurrently, by 2050, the proportion of urban residents is projected to exceed 70% of the world's total population [2]. Urban population growth is associated with a continuous increase in artificial impervious surfaces that alter the original land cover, especially in metropolises undergoing rapid economic development [3], [4], [5]. Meanwhile, impervious surfaces such as asphalt and cement contribute to a large increase in surface temperature, resulting the frequent occurrence of urban heat island (UHI) effect, which exacerbates the impact of heat waves and promotes extreme heat events, thereby affecting human well-being and productivity [6], [7], [8], [9]. Therefore, further research is required to investigate the underlying mechanisms of changes in the urban thermal environment and identify effective mitigation measures to further support sustainable development. Howard [10] was the first to report that urban temperatures are higher than suburban temperatures. Subsequently, Manley [11] defined this phenomenon as the UHI effect, while Oke [12] defined the difference between the maximum temperature of urban and suburban areas as the urban heat island intensity (UHII). These concepts attracted the attention of international scholars, who carried out a series of related studies [13], [14], [15]. With the continuous development of GIS and remote sensing technologies, which have many advantages compared with meteorological stations in terms of data collection, land surface temperature (LST) data obtained through remote sensing image data inversion has been widely used in UHI research because of its spatial continuity, wide time range coverage, and accessibility [16], [17], [18]]. In previous research on urban agglomerations or larger study areas, the data were mainly MODIS LST products; however, these images were excessively impacted by cloud cover, rendering them mostly unusable. In the study, the 1 km daily all-weather land surface temperature dataset was used (TRIMS LST) [19]. The spatiotemporal resolution of the dataset was high, and it was not greatly affected by weather conditions. The TRIMS LST dataset includes twice daily measurements of the overall LST distribution of a study area, which comprehensively reflects the spatiotemporal characteristics.

Manuscript received 10 January 2024; revised 17 February 2024; accepted 1 March 2024. Date of publication 5 March 2024; date of current version 22 March 2024. This work was supported in part by the National Natural Science Foundation of China under Grant 41771178, Grant 42030409, and Grant 41671151 and in part by the Fundamental Research Funds for the Central Universities under Grant N2111003. *(Corresponding author: Dongqi Sun.)*

Huisheng Yu is with the School of Management Engineering, Qingdao University of Technology, Qingdao 266520, China (e-mail: 901020230147@qut.edu.cn).

Dongqi Sun is with the Key Laboratory of Regional Sustainable Development Modeling, Institute of Geographic Sciences and Natural Resources Research, CAS, Beijing 100101, China (e-mail: sundq@igsnrr.ac.cn).

Digital Object Identifier 10.1109/JSTARS.2024.3373409

Recent research on urban thermal environments has mainly focused on three aspects: spatial and temporal distribution characteristics, influencing factors, and mitigation strategies [20], [21], [22], [23]. In recent years, several scholars have found that increasing the urban greening rate as well as changing the color and materials of buildings, roofs, roads, and other artificial components can effectively mitigate warming resulting from UHIs [24], [25], [26]. However, these measures have been primarily concentrated in built-up urban areas. An in-depth study of the UHI effect found that the associated warming occurs both within the built-up urban area and in the suburbs surrounding the city. The UHI effect affected areas outside the built-up areas are defined as the surface urban heat island footprint (SUHIF) [27], [28]. In addition, Zhou et al. [29] found that the SUHIF can encompass an area several times the size of the city. However, recent research on the urban thermal environment has mainly focused on evaluating surface urban heat island intensity (SUHII). Meanwhile, the SUHIF has received minimal attention, and existing research has primarily focused on individual cities. Few studies have been conducted on SUHII and the factors influencing the SUHIF in cities of different sizes. Therefore, in this article, we analyzed the spatiotemporal variation in the SUHII and SUHIF in the BT urban agglomeration from 2005 to 2018.

The factors influencing the urban thermal environment are complex, and the level of consistency in the influencing mechanisms of UHI intensity and footprint requires further study. Accordingly, we comprehensively considered social, economic, and environmental perspectives and investigated the relationships between UHI intensity and footprint and the nighttime light index, GDP, total residential population (PPP), population density (PD), construction land area (CLA), enhanced vegetation index (EVI), and PM2.5. The results of regression analysis are significantly not equivalent to having a causal relationship, but a reasonable regression analysis still has statistical significance. Therefore, this article aims to further identify the potential mechanisms of urban thermal environment changes, and cannot determine the causal relationship between variables with real significance. Therefore, the objectives of this article were to: quantify the spatiotemporal distributions of UHI intensity and footprint, and analyze the regional differences in the UHI effect in the BTH urban agglomeration from 2005 to 2018. The results of this article provide a valuable reference for sustainable urban development and UHI mitigation measures.

II. Study Area and Data Sources

A. Study Area

The BTH urban agglomeration includes 13 cities located in the northern part of the North China Plain (37°24′–42°35′N, 113°30′–119°50′E), with a total area of approximately 218 000 km^2. The northwestern terrain is high in elevation, while the southeastern terrain is low. The region has a temperate continental monsoon climate with four distinct seasons. Beijing and Tianjin are municipalities located directly under central government control. Hebei Province includes the prefecture-level cities of Chengde, Shijiazhuang, Cangzhou, Baoding, Hengshui, Handan, Langfang, Tangshan, Qinhuangdao, Zhangjiakou, and Xingtai (see Fig. 1). Following the reform and "opening up" period, the BTH urban agglomeration developed rapidly, leading to economic growth in the surrounding areas. However, despite the social and economic benefits of rapid urbanization, this development has also resulted in an increasingly prominent surface UHI effect. Therefore, the spatiotemporal variation characteristics in the urban thermal environment and their driving factors must be analyzed to thoroughly identify the potential risk.

B. Data Sources

In this article, we mainly evaluated LST, digital elevation model (DEM), urban boundary, nighttime light, EVI, statistical (including PPP, PD, GDP and CLA), and PM2.5 data (all from 2005, 2010, 2015, and 2018). The data sources are listed in Table III, Appendix.

III. Methodology

A. Calculation of Surface Urban Heat Island Intensity

To determine the difference in LST between urban and suburban areas, we established a buffer zone based on the extracted urban boundary data using ArcGIS. The buffer distance was 20 km, and the buffer range extended to the suburbs. The SUHII was calculated according to (1) as follows:

$$\mathrm{SUHII} = \mathrm{T}_{\mathrm{urban}} - \mathrm{T}_{\mathrm{suburban}} \tag{1}$$

where $\mathrm{T}_{\mathrm{urban}}$ and $\mathrm{T}_{\mathrm{suburban}}$ are the average LST values of the urban and suburban areas, respectively.

B. Exponential Fitting Method

To evaluate the UHI effect along the urban–suburban gradient without considering the clear boundary between urban and nonurban areas, we analyzed the SUHIF using the exponential fitting method. The larger the SUHIF, the greater the impact of the UHI effect on the suburbs. We designated the built-up urban area as the boundary and used the multiring buffer tool in ArcMap 10.4 to establish a 30 km buffer with an interval of 1 km. In addition, the calculation method of Fu et al. [30] was utilized. The body of water and areas with a difference of more than 50 m from the average DEM of the built-up area were excluded. The average LST in each buffer ring was then calculated as ΔT. The average LST of the farthest three buffer rings was defined as the reference LST (T_{ref}) for non-urban areas [31]. The ΔT of each buffer zone was calculated using (2) as follows:

$$\Delta T = T - T_{\mathrm{ref}} \tag{2}$$

where T is the average LST of the built-up area and buffer zone. Using Origin software, the average LST in the 30 km buffer ring was fitted using an exponentially decreasing model

$$\Delta T = A_1 \times e^{-\frac{x}{t_1}} + y_0 \tag{3}$$

where $A_1$is the maximum LST difference between the urban and suburban areas, $1/t_1$ is the LST decline rate, and y_0 is the

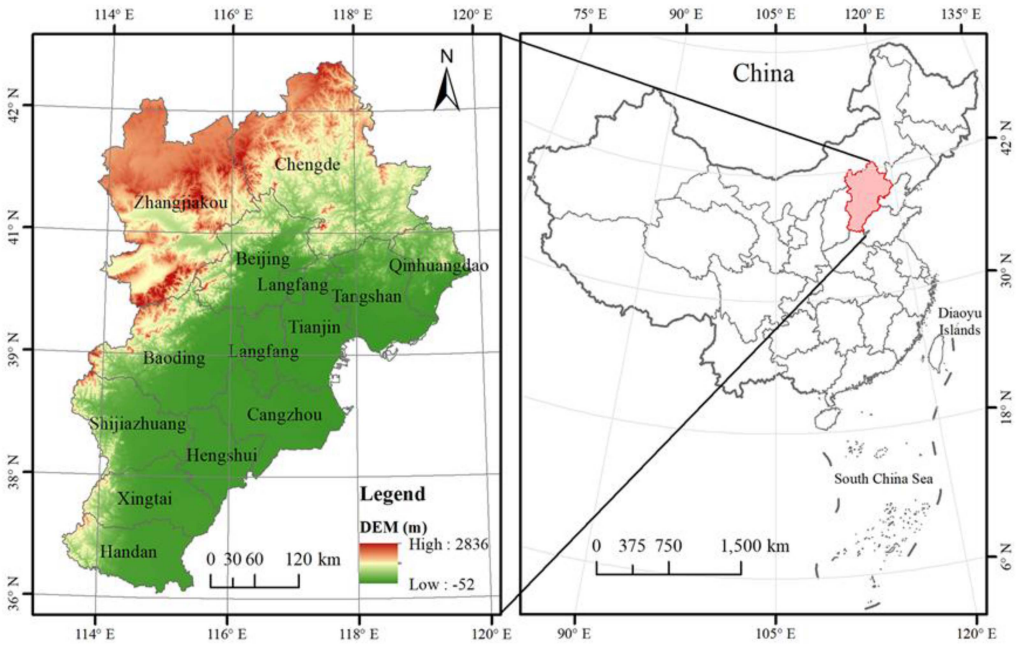

Fig. 1. Overview of the study area.

asymptotic value that can be acquired from the exponential trend. In this article, the SUHIF was determined based on the distance (D) from each exponential model to its 95% asymptotic value (i.e., y_0) [32].

However, previous studies and preliminary calculations revealed that, when using the exponential fitting method [33], the distance (D) value could not be fitted and the LST trend was inconsistent. Therefore, we examined and corrected the exponential fitting results of 13 cities as follows. When the LST change trend exponentially decreased and the average LST in the buffer zone differed by 0.1°C from the regional background temperature, the footprint was considered stable; concurrently, when $0 < D \leq 30$, the 95% confidence interval is met, and the Eq. (3) to calculate D is used. When the LST change trend exponentially increased, the distance d_1 of the first inflection point in the overall trend of LST was defined as D. In addition, when the trend of LST change reflected other complex trends, the distance d_1 of the first inflection point under the overall trend of LST was nonetheless set as D. The inflection point was defined as follows: based on the 95% confidence interval of the fitting curve, if there were data points outside the confidence interval, the trend of these data points was no longer considered in accordance with the exponentially decreasing trend, and the first concave or convex point in these data points was considered as the inflection point.

C. Multiple Linear Regression Analysis

Multiple linear regression refers to the number of independent variables with a linear correlation with a dependent variable greater than or equal to two

$$Y = b + a_1X_1 + a_2X_2 + a_3X_3 + \cdots + a_nX_n \quad (4)$$

where b, a_1, a_2, $a_3 \cdots a_n$ are regression coefficients; X_1, X_2, $X_3 \cdots X_n$ are independent variables; and Y is the dependent variable. The model-fitting effect was determined by analyzing the R^2 and P values, and the result of the multiple linear regression analysis was obtained.

IV. Results

A. Spatiotemporal Distribution of Surface Urban Heat Island Intensity

Based on the urban–suburban dichotomy, we calculated the daytime and nighttime SUHII spatial distribution maps of the BTH urban agglomeration in four research periods (see Figs. 2 and 3). We found that compared with the night, the diurnal average SUHII values were higher. From 2005 to 2018, the maximum daytime values of SUHII all occurred in Beijing, and the values all were greater than 3°C. By contrast, the maximum nighttime SUHII value occurred in Zhangjiakou, and all cities had values between 2 and 3°C. In addition, the average daytime SUHII values in 2005, 2010, 2015, and 2018 were 0.21°C, 0.03°C, 0.35°C, and 0.53°C higher than those at night, respectively.

As shown in Fig. 2, the maximum daytime value of SUHII from 2005 to 2018 were all occurred in Beijing and exhibited a gradual upward trend. The minimum values occurred in Langfang. In addition, high SUHII values were mainly concentrated in larger urban areas, such as Beijing and Tianjin. The reason for the higher SUHII values in Zhangjiakou and Chengde may be that we defined a range of 20 km from the built-up area as suburbs; however, this boundary covers several mountains, which likely influenced the difference in surface temperatures. Regarding temporal changes, the annual average values of the daytime SUHII in Beijing and Baoding showed a gradual upward trend from 2005 to 2018. The annual average daytime values of SUHII in Langfang were less than 0°C during 2005–2018,

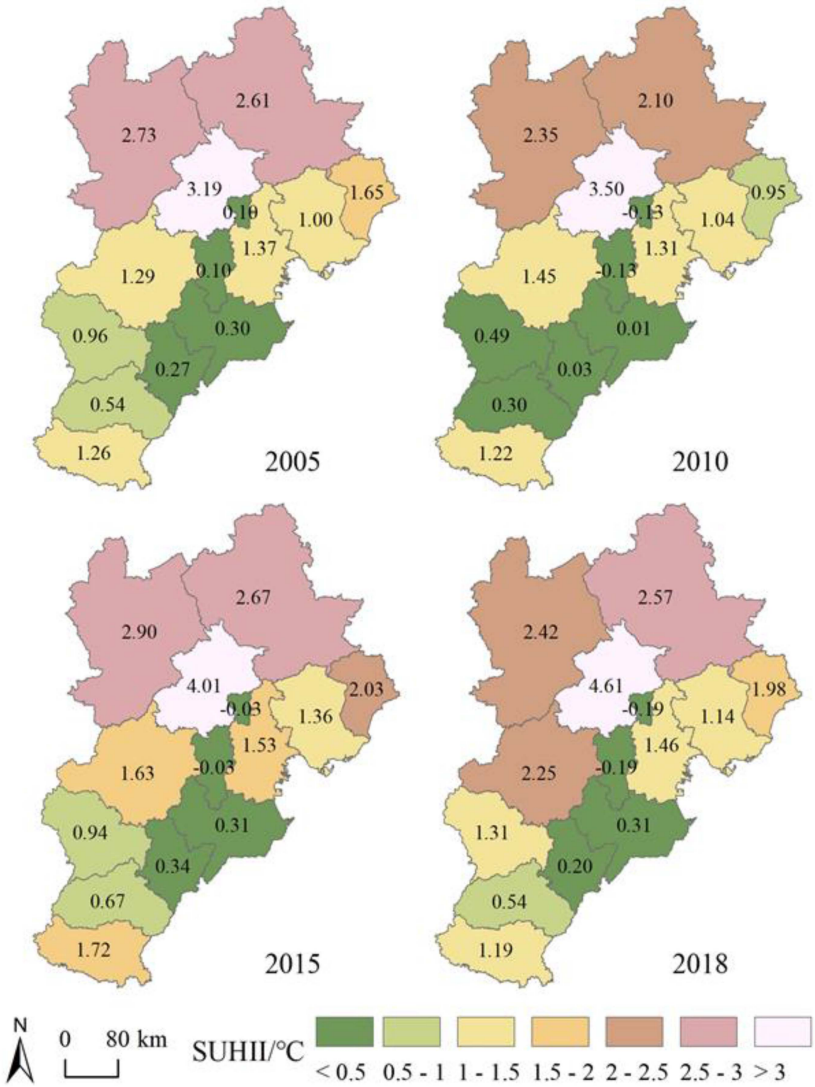

Fig. 2. Daytime UHI intensity distribution in the BTH urban agglomeration from 2005 to 2018.

indicating that an urban cold island appeared. This was mainly because the speed of the urbanization accelerated after 2010, and a large increase in CLA, which was affected by surrounding cities, such as Beijing and Tianjin, resulting in a general increase in temperature in the suburbs and the formation of urban cold islands (which means that the urban is cooler than the suburbs). The annual average daytime SUHII in Shijiazhuang first decreased from 2005 to 2010 and then increased from 2010 to 2018. For other cities, the annual average value of SUHII was largest in 2015 and smallest in 2010. The southward movement of Arctic cold air in 2009 also had a certain weakening effect on SUHII, whereas the decline in SUHII values in 2018 was closely related to the implementation of "ecological civilization" initiatives in China.

As shown in Fig. 3, the maximum nighttime values of SUHII during 2005–2018 occurred in Zhangjiakou. The minimum values were 0.32°C in Chengde in 2005, 0.39°C in Chengde in 2010, 0.59°C in Chengde in 2015, and 0.36°C in Cangzhou in 2018. An in-depth analysis revealed that high SUHII values at night were mainly concentrated in higher latitude areas. From 2005 to 2018, the annual average nighttime values of SUHII in all cities were greater than 0°C. The annual average nighttime SUHII values in Beijing and Tianjin showed a decreasing trend. The values in Chengde, Handan, and Xingtai showed an upward trend before 2015 and a downward trend after 2015. For the other cities, the overall trend fluctuated.

B. Spatiotemporal Distribution of Surface Urban Heat Island Footprint

We calculated the SUHIF with the single exponential decline model using Origin software, and the results are shown in Figs. 4 and 5. The results of the SUHIF single-index fitting model are shown in Appendix. The exponential decline proportion was 44.2%, the exponential increase proportion was 13.5%, and the proportion of other trends was 42.3%. The daytime and nighttime SUHIF values for each city were inconsistent in different years; however, the maximum values of this metric

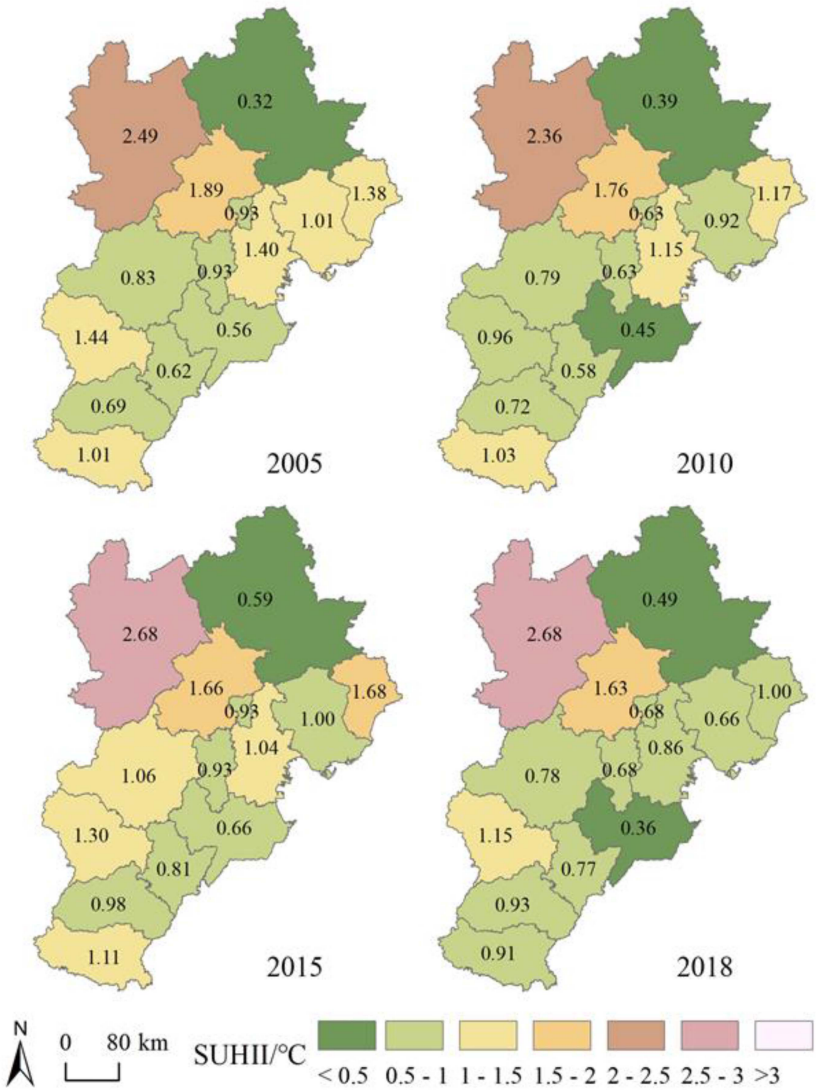

Fig. 3. Nighttime UHI intensity distribution in the BTH urban as from 2005 to 2018.

were mainly concentrated in densely populated areas, such as Beijing, Tianjin, Shijiazhuang, and Baoding, whereas the minimum values were mainly concentrated in Hengshui and Langfang. Although the population densities of Hengshui and Langfang were large, their construction land and research scope areas were small, which represents the main reason for their small heat island footprints. For example, in Beijing, the SUHIF was higher at night than during the day in 2005, whereas in 2010, 2015, and 2018, the opposite result was observed; in Tianjin, the SUHIF was higher at night than during the day in 2005 and 2015, with opposite result in 2010 and 2018.

During the daytime, the maximum heat island footprint areas in 2005, 2010, 2015, and 2018 were observed in Tianjin (13.47 km), Shijiazhuang (8.00 km), Shijiazhuang (8.00 km), and Beijing (7.74 km), and the minimum values were observed in Handan (2.24 km), Hengshui (2.55 km), Hengshui (1.58 km), and Langfang (2.00 km) (see Fig. 4). The footprint areas in Zhangjiakou, Xingtai, and Baoding first increased and then decreased, and the inflection point occurred in 2010. This may be because the cold air moving southward in 2009 also affected the outward diffusion of the heat island effect. The footprints of Shijiazhuang and Chengde first increased and then decreased, and an inflection point occurred in 2015. This was likely related to China's emphasis on "ecological civilization" construction in 2018. Qinhuangdao's footprint showed a gradual downward trend; the footprints of Tangshan and Hengshui first decreased and then increased, with an inflection point in 2015; those of Tianjin, Langfang, Cangzhou, and Beijing fluctuated; and that of Handan showed a gradually increasing trend. This was mainly because of the rapid development of Handan from 2005 to 2018 and the increasing PD, which suggests that human factors can strongly enhance the heat island effect.

C. Influence of Regional Differences on Urban Heat Island Intensity

From 2005 to 2018, the results of principal component analysis showed that the first three principal components of both day

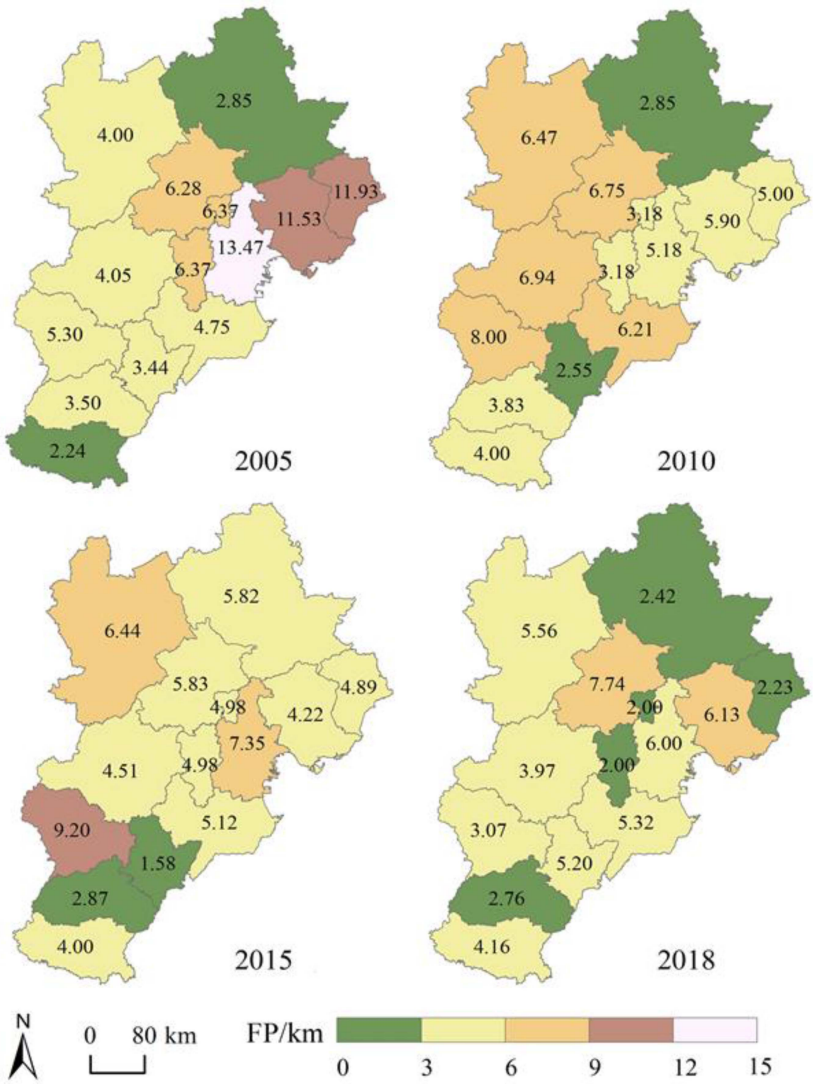

Fig. 4. Daytime UHI footprint distribution in the BTH urban agglomeration from 2005 to 2018. FP represents the UHI footprint.

and night (PD, PM2.5, and EVI) contained more than 85% of the information found in the original variables. Therefore, a factor load-coefficient table was calculated for these components. In this article, PD, EVI, and PM2.5 were selected for subsequent multiple linear regression analysis. The daytime variance inflation factor (VIF) values in 2005, 2010, 2015, and 2018 were all less than 10; therefore, the model had no multicollinearity problems and was properly constructed. The R^2 values (adjusted values) in 2005, 2010, 2015, and 2018 were 0.863 (0.818), 0.834 (0.779), 0.831 (0.775), and 0.745 (0.659), respectively (see Fig. 6). The fitting results passed the confidence test at the $P = 0.01$ level. Therefore, the proposed model met these requirements. Regarding the nighttime data for 2005, 2010, 2015, and 2018, although the VIF was less than 10, excluding the multicollinearity of impact factors, the R^2 values were small, the fitting results were poor, and the P value did not pass the F test; thus, the model was invalid. Therefore, a multiple linear regression model was established between daytime SUHII and PM2.5, EVI, and PD in 2005, 2010, 2015, and 2018. The results (see Table I) showed a negative correlation between PM2.5 and SUHII, and positive correlations between PD and SUHII and between EVI and SUHII.

TABLE I
NORMALIZED COEFFICIENT TABLE OF LINEAR REGRESSION ANALYSIS (SUHII)

	2005D	2005N	2010D	2010N	2015D	2015N	2018D	2018N
PM2.5	−1.509	−0.628	−1.672	−0.858	−1.455	−0.673	−1.265	−0.504
PD	0.797	0.479	1.14	0.621	0.832	0.269	0.869	0.121
EVI	0.259	−0.349	0.211	−0.234	0.275	−0.183	0.475	−0.037

D. Impact of Regional Differences on Urban Heat Island Footprint

Considering that SUHII and SUHIF have the same influencing factors, the results of principal component analysis were the same and are not repeated here. Based on the multiple linear regression calculation, although the VIF values for each year were less than 10, there was no multicollinearity problem; except for that of the nighttime data from 2015, the adjusted R^2 values

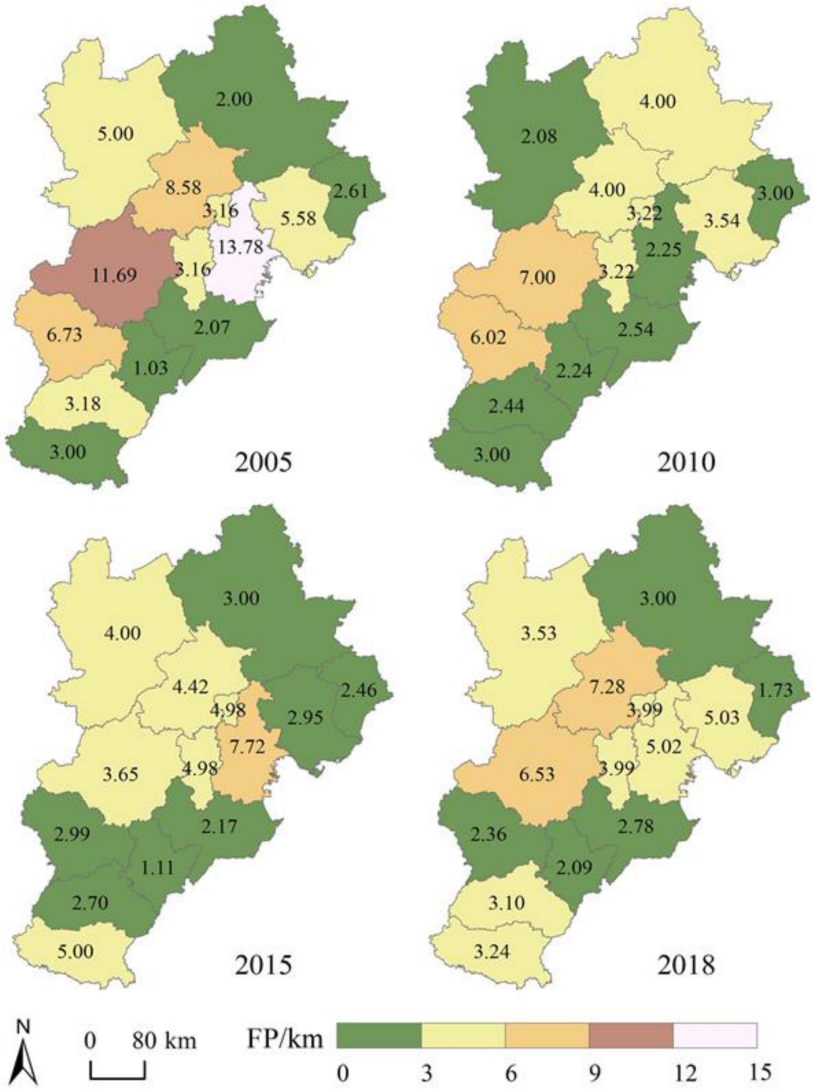

Fig. 5. Nighttime UHI footprint distribution in the BTH urban agglomeration from 2005 to 2018. FP represents the UHI footprint.

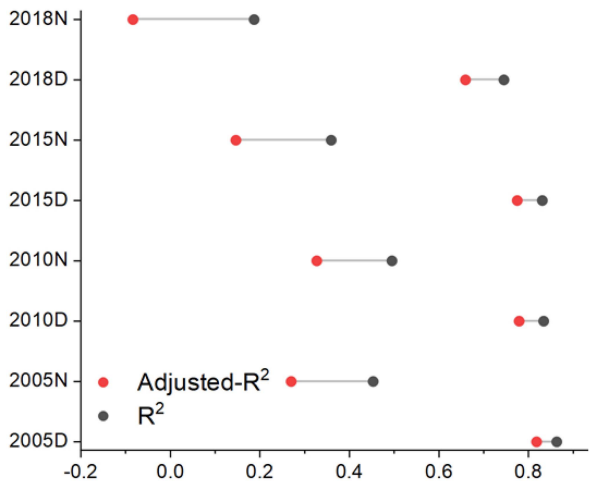

Fig. 6. Linear fitting results of daytime and nighttime heat island intensity in the BTH urban agglomeration during 2005–2018.

TABLE II
NORMALIZED COEFFICIENT TABLE OF LINEAR REGRESSION ANALYSIS (SUHIF)

	2005D	2005N	2010D	2010N	2015D	2015N	2018D	2018N
PM2.5	−0.355	−0.433	−0.031	−0.292	−0.761	−0.523	−0.454	−0.795
PD	0.562	0.798	0.226	0.291	0.683	0.875	0.552	0.972
EVI	−0.416	−0.376	−0.489	0.182	−0.289	−0.452	−0.196	0.098

of the other years were low (see Fig. 7) and did not pass the significance test ($P < 0.01$). Thus, the model was invalid. The R^2 value of the nighttime data from 2015 was 0.672, the adjusted R^2 value was 0.562, and the confidence test was passed at the $P < 0.01$ level, indicating that the model met the requirements. Therefore, we established a multiple linear regression model between SUHIF and PM2.5, PD, and EVI for nighttime data in 2015. The coefficients of PM2.5, PD, and EVI were -0.523, 0.875, and -0.452, respectively, indicating that PM2.5 and EVI were negatively correlated with SUHIF (see Table II).

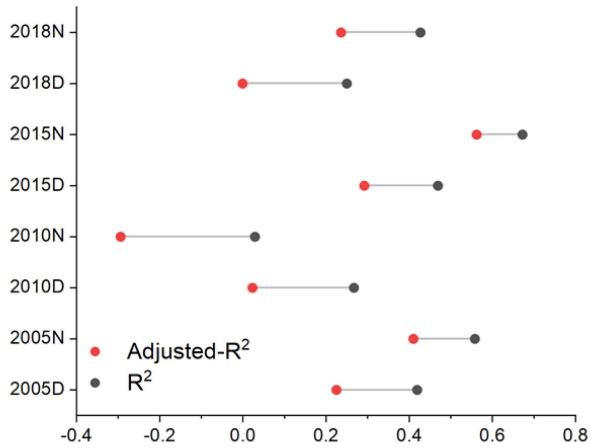

Fig. 7. Linear fitting results of daytime and nighttime heat island footprint in the BTH urban agglomeration during 2005–2018.

V. Discussion

We calculated the SUHII and SUHIF of the BTH urban agglomeration based on TRIMS LST data and analyzed the influence of social, economic, and environmental factors on regional differences in heat island intensity and footprint in the Beijing–Tianjin–Hebei urban agglomeration from 2005 to 2018. The results revealed that the daytime SUHII values were higher than the nighttime values, and the high SUHII values were concentrated in lower latitude areas [14], [34], [35], [36]. Furthermore, high SUHII and SUHIF values were concentrated in areas with a large city size and high PD. With the exception of the values in rapidly developing cities, such as Beijing, SUHII and SUHIF values showed the lowest trends in 2010 and the highest trends in 2015, which were likely associated with the southward movement of Arctic cold air in 2009 and its accumulation in North China, the acceleration of urbanization, and the emphasis on ecological civilization construction in 2018.

Based on the results of principal component analysis, the influence of PD, PM2.5, and EVI on SUHII and SUHIF were analyzed using multiple linear regression. The results showed that PM2.5 was negatively correlated with SUHII and SUHIF. This may be due to the scattering and absorption of solar radiation by aerosols, which can lead to a reduction in LST. Notably, the concentration of PM2.5 was consistently higher in urban areas than in suburban areas, so the cooling effect was greater in urban areas [37], [38], [39], [40]. Meanwhile, PD was positively correlated with SUHII and SUHIF. This is because during urbanization, the area of impervious surfaces that cover the surface vegetation increases, thereby decreasing surface reflectance and causing more solar radiation to be absorbed, which further increases the LST[41], [42]. Simultaneously, an increase in PD causes an increase in anthropogenic heat, resulting in an increase in LST [43]. However, the EVI was positively correlated with SUHII and negatively correlated with SUHIF. When calculating the driving factors of SUHII and SUHIF, we found that nighttime values were more susceptible to PD and daytime values were more susceptible to PM2.5. The correlations between SUHII and SUHIF and their driving factors were somewhat inconsistent. Thus, measures for alleviating the UHI effect should be based on the actual situation of an area rather than on generalizations.

Using the daily 1 km all-weather surface temperature dataset (TRIMS LST) from China's land and surrounding areas to compensate for the lack of data in the MODIS series products. At the same time, considering heat island intensity and heat island footprint, the heat island effect and regional differences in the Beijing Tianjin Hebei urban agglomeration were quantified, providing important reference value for improving urban climate. Although this article revealed the spatiotemporal variations in SUHII and SUHIF in the BTH urban agglomeration from 2005 to 2018, some limitations remain. First, when calculating the heat island intensity and footprint, the TRIMS LST of China's land and surrounding areas was used, leading to some errors in the analysis results at the city scale. Second, common methods for calculating the heat island intensity and footprint were used in this article, and there was a lack of comparison of different methods. Finally, the selection of the driving factors in this article was based on previous research, and many influencing factors have yet to be verified. Therefore, future studies should address these limitations.

VI. Conclusion

Based on the TRIMS LST dataset for China and its surrounding areas, we employed the exponential fitting method and conducted principal component analysis and multiple linear regression to analyze the spatiotemporal distribution and driving factors of UHII and UHIF. We drew the following conclusions.

1) Overall, the SUHII values during the day were higher than those at night. The maximum value of SUHII was observed in Beijing, and all cities showed values greater than 3°C. From 2005 to 2018, an increasing trend also occurred annually. The maximum nighttime SUHII values from 2005 to 2018 occurred in Zhangjiakou, and all cities showed values between 2 and 3°C. The diurnal SUHII difference also showed an increasing trend, with differences of 0.70°C, 1.14°C, 1.33°C, and 1.93°C in 2005, 2010, 2015, and 2018, respectively.
2) During the day, the maximum heat island footprints in 2005, 2010, 2015, and 2018 were in Tianjin (13.47 km), Shijiazhuang (8.00 km), Shijiazhuang (8.00 km), and Beijing (7.74 km), respectively. The minimum heat island footprints were in Handan (2.24 km), Hengshui (2.55 km), Hengshui (1.58 km), and Langfang (2.00 km), respectively. At night, the maximum heat island footprint values in 2005, 2010, 2015, and 2018 were in Tianjin (13.78 km), Baoding (7.00 km), Tianjin (7.72 km), and Beijing (7.28 km), and the minimum values were in Hengshui (1.03 km), Zhangjiakou (2.08 km), Hengshui (1.11 km), and Qinhuangdao (1.73 km), respectively.
3) In 2005, 2010, 2015, and 2018, PM2.5 was negatively correlated with daytime SUHII, while PD and EVI were positively correlated with daytime SUHII.
4) In 2015, PM2.5 and EVI were negatively correlated with nighttime SUHIF, whereas PD was positively correlated with SUHIF. However, the model results for the influencing factors of SUHII and SUHIF at other times were poor.

APPENDIX

TABLE III
A BRIEF INTRODUCTION TO THE DATA SOURCES AND PREPROCESSING PROCESS

Data type	Data	Time	Resolution	Data source
Land surface temperature	Daily 1 km all-weather LST data set in China and its surrounding areas TRIMS LST	2005–2018	1 km	National Qinghai-Tibet Plateau Scientific Data Center http://data.tpdc.ac.cn/zh-hans/
DEM	SRTMDEM	-	90 m	Geographical spatial data cloud http://www.gscloud.cn/
Administrative division data	-	2019	-	Geographical spatial data cloud http://www.gscloud.cn/
Urban boundary data	GUB	2005–2018	30 m	Global Urban Boundary Dataset http://data.ess.tsinghua.edu.cn/gub.html
Nighttime lighting data	NPP-VIIRS	2005–2018	750 m	NCEI National Environmental Information Center Earth Observation Group https://payneinstitute.mines.edu/eog/
Vegetation index data	MYD13A2	2005–2018	1 km	Level 1 Atmospheric Archives and Distribution System Distributed Activity Archives Center https://ladsweb.modaps.eosdis.nasa.gov/search/
Statistical Yearbook data	GDP, total residential population, population density and construction, land area	2005–2018	-	China knowledge network https://www.cnki.net/
Air quality data	$PM_{2.5}$	2005–2018	-	https://zenodo.org/record/6372847

REFERENCES

[1] UN-Habitat *World Cities Report 2020—The Value of Sustainable Urbanization | UN-Habitat*. Nairobi, Kenya: UN-Habitat, 2020, vol. 51.

[2] M. O. Sarif, B. Rimal, and N. E. Stork, "Assessment of changes in land use/land cover and land surface temperatures and their impact on surface urban heat island phenomena in the Kathmandu Valley (1988–2018)," *ISPRS Int. J. Geo-Inf.*, vol. 9, no. 12, Dec. 2020, Art. no. 12, doi: 10.3390/ijgi9120726.

[3] T. Panagopoulos, J. A. González Duque, and M. Bostenaru Dan, "Urban planning with respect to environmental quality and human well-being," *Environ. Pollut.*, vol. 208, pp. 137–144, Jan. 2016, doi: 10.1016/j.envpol.2015.07.038.

[4] A. Dewan, G. Kiselev, D. Botje, G. I. Mahmud, M.. H. Bhuian, and Q. K. Hassan, "Surface urban heat island intensity in five major cities of Bangladesh: Patterns, drivers and trends," *Sustain. Cities Soc.*, vol. 71, pp. 102926, Aug. 2021, doi: 10.1016/j.scs.2021.102926.

[5] J. S. Silva, R. M. da Silva, and C. A. G. Santos, "Spatiotemporal impact of land use/land cover changes on urban heat islands: A case study of Paço do Lumiar, Brazil," *Building Environ.*, vol. 136, pp. 279–292, May 2018, doi: 10.1016/j.buildenv.2018.03.041.

[6] A. Hsu, G. Sheriff, T. Chakraborty, and D. Manya, "Disproportionate exposure to urban heat island intensity across major US cities," *Nat. Commun.*, vol. 12, no. 1, May 2021, Art. no. 2721, doi: 10.1038/s41467-021-22799-5.

[7] S. A. Lowe, "An energy and mortality impact assessment of the urban heat island in the US," *Environ. Impact Assessment Rev.*, vol. 56, pp. 139–144, Jan. 2016, doi: 10.1016/j.eiar.2015.10.004.

[8] R. Zhang, "Cooling effect and control factors of common shrubs on the urban heat island effect in a southern city in China," *Sci. Rep.*, vol. 10, no. 1, Oct. 2020, Art. no. 17317, doi: 10.1038/s41598-020-74559-y.

[9] Z. Zhao, A. Sharifi, X. Dong, L. Shen, and B.-J. He, "Spatial variability and temporal heterogeneity of surface urban heat island patterns and the suitability of local climate zones for land surface temperature characterization," *Remote Sens.*, vol. 13, no. 21, Jan. 2021, Art. no. 21, doi: 10.3390/rs13214338.

[10] L. Howard, "The Climate of London: Deduced from Meteorological Observations, vol. 1," in *Cambridge Library Collection - Earth Science*, vol. 1. Cambridge, MA, USA: Cambridge Univ. Press, 2012. doi: 10.1017/CBO9781139226899.

[11] G. Manley, "On the frequency of snowfall in metropolitan England," *Quart. J. Roy. Meteorol. Soc.*, vol. 84, no. 359, pp. 70–72, Jan. 1958, doi: 10.1002/qj.49708435910.

[12] T. R. Oke, "The energetic basis of the urban heat island," *Quart. J. Roy. Meteorol. Soc.*, vol. 108, no. 455, pp. 1–24, Jan. 1982, doi: 10.1002/qj.49710845502.

[13] B. Yang et al., "Traffic restrictions during the 2008 Olympic Games reduced urban heat intensity and extent in Beijing," *Commun Earth Environ*, vol. 3, no. 1, pp. 1–10, May 2022.

[14] J. Yang, J. Xin, Y. Zhang, X. Xiao, and J. C. Xia, "Contributions of sea–land breeze and local climate zones to daytime and nighttime heat island intensity," *NPJ Urban Sustain.*, vol. 2, no. 1, pp. 1–11, May 2022, doi: 10.1038/s42949-022-00055-z.

[15] M. F. Baqa et al., "Characterizing spatiotemporal variations in the urban thermal environment related to land cover changes in Karachi, Pakistan, from 2000 to 2020," *Remote Sens.*, vol. 14, no. 9, Jan. 2022, Art. no. 2164, doi: 10.3390/rs14092164.

[16] D. E. Okumus and F. Terzi, "Evaluating the role of urban fabric on surface urban heat island: The case of Istanbul," *Sustain. Cities Soc.*, vol. 73, Oct. 2021, Art. no. 103128, doi: 10.1016/j.scs.2021.103128.

[17] S. Haashemi, Q. Weng, A. Darvishi, and S. K. Alavipanah, "Seasonal variations of the surface urban heat island in a semi-arid City," *Remote Sens.*, vol. 8, no. 4, Apr. 2016, Art. no. 352, doi: 10.3390/rs8040352.

[18] D. Zhou, S. Zhao, S. Liu, L. Zhang, and C. Zhu, "Surface urban heat island in China's 32 major cities: Spatial patterns and drivers," *Remote Sens. Environ.*, vol. 152, pp. 51–61, Sep. 2014, doi: 10.1016/j.rse.2014.05.017.

[19] W. Tang et al., "TRIMS LST: A daily 1-km all-weather land surface temperature dataset for the Chinese landmass and surrounding areas (2000-2021)," *Earth Syst.Sci. Data Discuss.*, pp. 1–34, Mar. 2023, doi: 10.5194/essd-2023-27.

[20] F. Cui et al., "Quantifying the response of surface urban heat island to urban greening in global north megacities," *Sci. Total Environ.*, vol. 801, Dec. 2021, Art. no. 149553, doi: 10.1016/j.scitotenv.2021.149553.
[21] H. Du et al., "Influences of land cover types, meteorological conditions, anthropogenic heat and urban area on surface urban heat island in the Yangtze River Delta Urban Agglomeration," *Sci. Total Environ.*, vol. 571, pp. 461–470, Nov. 2016, doi: 10.1016/j.scitotenv.2016.07.012.
[22] D. Han, H. An, H. Cai, and F. Wang, "How do 2D/3D urban landscapes impact diurnal land surface temperature: Insights from block scale and machine learning algorithms," *Sustain. Cities Soc.*, vol. 99, Dec. 2023, Art. no. 104933, doi: 10.1016/j.scs.2023.104933.
[23] D. Han, X. Xu, Z. Qiao, and F. Wang, "The roles of surrounding 2D/3D landscapes in park cooling effect: Analysis from extreme hot and normal weather perspectives," *Building Environ.*, vol. 231, Mar. 2023, Art. no. 110053, doi: 10.1016/j.buildenv.2023.110053.
[24] H. Farhadi, M. Faizi, and H. Sanaieian, "Mitigating the urban heat island in a residential area in Tehran: Investigating the role of vegetation, materials, and orientation of buildings," *Sustain. Cities Soc.*, vol. 46, pp. 101448, Apr. 2019, doi: 10.1016/j.scs.2019.101448.
[25] T. Susca, S. R. Gaffin, and G. R. Dell'Osso, "Positive effects of vegetation: Urban heat island and green roofs," *Environ. Pollut.*, vol. 159, no. 8, pp. 2119–2126, Aug. 2011, doi: 10.1016/j.envpol.2011.03.007.
[26] N. H. Wong, C. L. Tan, D. D. Kolokotsa, and H. Takebayashi, "Greenery as a mitigation and adaptation strategy to urban heat," *Nat. Rev. Earth Environ.*, vol. 2, no. 3, Mar. 2021, Art. no. 3, doi: 10.1038/s43017-020-00129-5.
[27] X. Fu, L. Yao, and S. Sun, "Accessing the heat exposure risk in Beijing–Tianjin–Hebei region based on heat island footprint analysis," *Atmosphere*, vol. 13, no. 5, May 2022, Art. no. 739, doi: 10.3390/atmos13050739.
[28] J. Hu, Y. Yang, Y. Zhou, T. Zhang, Z. Ma, and X. Meng, "Spatial patterns and temporal variations of footprint and intensity of surface urban heat island in 141 China cities," *Sustain. Cities Soc.*, vol. 77, Feb. 2022, Art. no. 103585, doi: 10.1016/j.scs.2021.103585.
[29] D. Zhou, S. Zhao, L. Zhang, G. Sun, and Y. Liu, "The footprint of urban heat island effect in China," *Sci. Rep.*, vol. 5, no. 1, Jun. 2015, Art. no. 11160, doi: 10.1038/srep11160.
[30] X. Fu, L. Yao, W. Xu, Y. Wang, and S. Sun, "Exploring the multitemporal surface urban heat island effect and its driving relation in the Beijing-Tianjin-Hebei urban agglomeration," *Appl. Geogr.*, vol. 144, Jul. 2022, Art. no. 102714, doi: 10.1016/j.apgeog.2022.102714.
[31] J. Martin-Vide, P. Sarricolea, and M. C. Moreno-García, "On the definition of urban heat island intensity: The 'rural' reference," *Front. Earth Sci.*, vol. 3, 2015, Accessed: Jan. 8, 2024, Art. no. 24. [Online]. Available: https://www.frontiersin.org/articles/10.3389/feart.2015.00024
[32] X. Zhang, M. A. Friedl, C. B. Schaaf, A. H. Strahler, and A. Schneider, "The footprint of urban climates on vegetation phenology," *Geophys. Res. Lett.*, vol. 31, no. 12, Jun. 2004, Art. no. 2004GL020137, doi: 10.1029/2004GL020137.
[33] M. Sun, *Simulating Urban Heat Island Footprint Using Machine Learning and Land Surface Temperature Data*. Lanzhou,China: Lanzhou Univ., 2020.
[34] N. Hu, Z. Ren, and Y. Dong, "Spatiotemporal evolution of heat island effect and its driving factors in urban agglomerations of China," *Scientia Geographica Sinica*, vol. 42, no. 9, pp. 1534–1545, 2022, doi: 10.13249/j.cnki.sgs.2022.09.003.
[35] X. Zhang, X. Wang, and Y. Zheng, "Effects of aerosol optical depth and impervious surface percenttage on urban heat island intensity: A case study in Guanzhong Region," *Acta Ecoligica Sinica*, vol. 41, pp. 8965–8976, 2021.
[36] Y. Cui, D. Yan, T. Hong, and J. Ma, "Temporal and spatial characteristics of the urban heat island in Beijing and the impact on building design and energy performance," *Energy*, vol. 130, pp. 286–297, Jul. 2017, doi: 10.1016/j.energy.2017.04.053.
[37] H. Wu, T. Wang, N. Riemer, P. Chen, M. Li, and S. Li, "Urban heat island impacted by fine particles in Nanjing, China," *Sci. Rep.*, vol. 7, no. 1, Sep. 2017, Art. no. 1, doi: 10.1038/s41598-017-11705-z.
[38] M. Jin and R. E. Dickinson, "Land surface skin temperature climatology: Benefitting from the strengths of satellite observations," *Environ. Res. Lett.*, vol. 5, no. 4, 2010, Art. no. 044004, doi: 10.1088/1748-9326/5/4/044004.
[39] D. Li, S. Malyshev, and E. Shevliakova, "Exploring historical and future urban climate in the Earth System modeling framework: 2. Impact of urban land use over the continental United States," *J. Adv. Model. Earth Syst.*, vol. 8, no. 2, pp. 936–953, 2016, doi: 10.1002/2015MS000579.
[40] D. Zhou, L. Zhang, D. Li, D. Huang, and C. Zhu, "Climate–vegetation control on the diurnal and seasonal variations of surface urban heat islands in China," *Environ. Res. Lett.*, vol. 11, no. 7, 2016, Art. no. 074009, doi: 10.1088/1748-9326/11/7/074009.
[41] E. Morini, B. Castellani, S. De Ciantis, E. Anderini, and F. Rossi, "Planning for cooler urban canyons: Comparative analysis of the influence of façades reflective properties on urban canyon thermal behavior," *Sol. Energy*, vol. 162, pp. 14–27, Mar. 2018, doi: 10.1016/j.solener.2017.12.064.
[42] E. Morini, A. G. Touchaei, F. Rossi, F. Cotana, and H. Akbari, "Evaluation of albedo enhancement to mitigate impacts of urban heat island in Rome (Italy) using WRF meteorological model," *Urban Climate*, vol. 24, pp. 551–566, Jun. 2018, doi: 10.1016/j.uclim.2017.08.001.
[43] S. A. Benz, P. Bayer, and P. Blum, "Identifying anthropogenic anomalies in air, surface and groundwater temperatures in Germany," *Sci. Total Environ.*, vol. 584–585, pp. 145–153, Apr. 2017, doi: 10.1016/j.scitotenv.2017.01.139.

Huisheng Yu received the Ph.D. degree in land resource management from the Northeast University of China, Shenyang, China, in 2023.

He is currently a Lecturer with the School of Management Engineering, Qingdao University of Technology, Qingdao, China. He has committed to urban spatial growth and its ecological and environmental effects, as well as urban climate.

Dongqi Sun received the Ph.D. degree in urban and regional planning from Nanjing University, Nanjing, China, in 2014.

He is currently an Associate Researcher with the Key Laboratory of Regional Sustainable Development Modeling, Institute of Geographic Sciences and Natural Resources Research, Chinese Academy of Sciences, Beijing, China. He has committed to economic geography and regional planning.